

# Materials Advances

Accepted Manuscript

This article can be cited before page numbers have been issued, to do this please use: T. Ishaq, R. Sattar, R. Naeem, M. Iqbal and S. Ullah, *Mater. Adv.*, 2026, DOI: 10.1039/D5MA01178G.



This is an Accepted Manuscript, which has been through the Royal Society of Chemistry peer review process and has been accepted for publication.

Accepted Manuscripts are published online shortly after acceptance, before technical editing, formatting and proof reading. Using this free service, authors can make their results available to the community, in citable form, before we publish the edited article. We will replace this Accepted Manuscript with the edited and formatted Advance Article as soon as it is available.

You can find more information about Accepted Manuscripts in the [Information for Authors](#).

Please note that technical editing may introduce minor changes to the text and/or graphics, which may alter content. The journal's standard [Terms & Conditions](#) and the [Ethical guidelines](#) still apply. In no event shall the Royal Society of Chemistry be held responsible for any errors or omissions in this Accepted Manuscript or any consequences arising from the use of any information it contains.

## RESEARCH ARTICLE

## Designing PANI modified PU films coupled with CNTs for the enhanced shape memory properties

Tehmeena Ishaq,<sup>a</sup> Rabia Sattar,<sup>\*a</sup> Rabia Naeem,<sup>\*b</sup> Mahwish Iqbal<sup>c</sup> and Sana Ullah<sup>d</sup>

Received 00th January 20xx,  
Accepted 00th January 20xx

DOI: 10.1039/x0xx00000x

Polyurethane (PU) based shape memory polymers are considered a supreme choice for shape recovery applications. However, they face problems with their mechanical and thermal properties which can lead to significant challenges in their development and practical implications. Herein, an effectual and novel strategy has been adopted to overcome these limitations by incorporating CNTs along with polyaniline to the PU chains to form a ternary PU-based nanocomposite. By introducing these conductive fillers, an exceptional elongation at break (18.35%), a higher thermal stability (up to 342°C), an optimal Young's Modulus (456.49 MPa) and high tensile strength (26.49 MPa) is achieved. However, a higher shape recovery aptitude (97%), higher shape fixity (98%) and an enhanced electrical conductivity of  $5.00 \times 10^{-2} \text{ S cm}^{-1}$  were achieved for the ternary hybrid. Overall, PANI/f-CNTs@PU nanocomposite designed in the current study depicted ideal shape memory parameters, which can be credited to the combined effect of the CNTs and PANI in the PU matrix. The fabricated nanocomposite PANI/f-CNTs@PU can be further utilized in various memory-based applications of materials in diversified industrial applications including sensors, self-healing materials and electronics, etc.

### 1. Introduction

The term "smart materials" dates back to the 1980s and it became the cornerstone of the modern industry owing to its huge variety of applications in the fields of robotics, aerospace, smart manufacturing, biomedicine, artificial intelligence, flexible electronics, etc. Smart composite materials are a class of novel materials that can make active responses when subjected to an external stimulus with the functions of self-healing, self-

<sup>a</sup>. Department of Chemistry, University of Lahore, Sargodha Campus, Sargodha 40100, Pakistan; [ishaqtehmeena@gmail.com](mailto:ishaqtehmeena@gmail.com); [rabiasattar39@yahoo.com](mailto:rabiasattar39@yahoo.com)

<sup>b</sup>. Department of Chemistry, Government College University Lahore, Katchery Road, 54000, Pakistan; [rabianaem@qcu.edu.pk](mailto:rabianaem@qcu.edu.pk)

<sup>c</sup>. Department of Chemistry, University of Agriculture, Faisalabad-38000, Pakistan; [mahwishiqbal2323@gmail.com](mailto:mahwishiqbal2323@gmail.com)

<sup>d</sup>. Nano Fusion Technology Research Group, Institute for Fiber Engineering (IFES), Interdisciplinary Cluster for Cutting Edge Research (ICCER), Shinshu University, Tokida 3-15-1, Ueda 386-8567, Nagano, Japan; [sana\\_ullah@shinshu-u.ac.jp](mailto:sana_ullah@shinshu-u.ac.jp)

† Footnotes relating to the title and/or authors should appear here.



deriving and self-sensing, etc.<sup>1</sup>. Smart structures and smart materials are machinable structural set-ups which incorporate sensing, control and actuate various functions. Shape memory polymers (SMPs) is a category of polymeric materials that manifest the unique capability to recover their original dimensions and permanent shape when stimulated by a specific external stimulus such as magnetism<sup>2</sup>, light<sup>3</sup>, electricity<sup>4</sup> or heat<sup>5</sup>. SMPs can be characterized by their versatile nature with regard to programmable deformation, easy molding, composability and stiffness<sup>6</sup>. SMPs include thermoplastic resins and thermosetting resins like polycaprolactone, polylactic acid, polystyrene, polyimide, cyanate ester<sup>7</sup>, elium<sup>8</sup>, epoxy resin, and polyurethane<sup>7</sup>. Among these SMPs, polyurethane (PU) stands out as a considerable choice as being a shape memory material for different applications due to its structural diversity and tunable nature. Although PU is well known for its higher melting point, easy manufacturing and excellent elasticity<sup>9</sup>. Even so, poor thermal and mechanical properties<sup>10</sup> can limit its usage at an industrial scale; however, these properties can be improved by incorporating suitable nanofillers in the polymeric matrix of the PU chains<sup>11</sup>. For instance, Baber et al.<sup>12</sup> reported Bentone/PU clay-based composite and observed 34% improvement in the glass transition temperature ( $T_g$ ) with a shift of degradation temperature to 46 °C compared to pristine PU. Furthermore, the effect of carbon nanotube (CNTs) in enhancing the shape recovery properties of SMPs has been investigated intensively for example, Gohar et al. reported the tensile strength of MWCNT@PU nanocomposite with 0-1.0 wt % loading of MWCNTs. It was revealed that elongation at break was improved by 11% while elastic modulus was increased by 25% and ultimate tensile strength was increased by about 21% for 1%MWCNT@PU composite compared to pristine PU<sup>13</sup>. This enhancement in strength and elastic modulus was ascribed to uniform dispersion and interfacial bonding between PU chains and MWCNTs. In another study, Namathoti et al.<sup>14</sup> reported an improvement in the thermal and tensile properties of HNT/MWCNTs@PU. The higher tensile value of 23.5 MPa while  $T_g$  at 69.0°C was observed for 0.1% MWCNTs loading in the PU matrix. Recently, interest in the PANI based conducting materials has been increased owing to its high environmental stability, effortless synthesis and higher electrical conductivity<sup>15, 16</sup>. In addition, there has been reports which manifest that polyaniline mixing with other polymers to form SMP composites, results in improvement of thermal, mechanical and electrical properties. For instance, Wang et al. designed HCNT/PANI/PU based composite via directional freezing and achieved a high degree of shape deformation and shape recovery which was credited to the hydrogen bonding developed between PU and PANI network<sup>17</sup>.

Although there have been many reports that reveal the positive impact of CNTs and PANI on the shape recovery properties of the PU, there is no reported work for the collective effect of the f-CNTs along with PANI on the shape memory properties of the PU matrix till date, to the best of

our knowledge. The aim of current study was to measure the impact of amine functionalized CNTs (f-CNTs) as well as PANI on the electrical, mechanical, thermal and shape recovery properties of the PU matrix by varying the concentration of PANI in the ternary composite material to achieve an optimized SMP which could be employed in the future for diverse shape memory applications with higher electrical conductivity and superior thermal stability at the industrial scale. Hence, our work investigates their combined impact on shape memory, electrical conductivity and mechanical integrity under controlled composition and concentration. Moreover, we demonstrated that low PANI content leads to a non-linear increase in shape memory properties. Additionally, our present work focuses on using a low amount of conductive fillers, non-toxic and cost-effective precursors for the SMPs and minimizing the harmful impact on the environment.

## 2 Material and methods

### 2.1 Chemicals Used

Polyethylene oxide (PEO, MW=10<sup>5</sup>), poly(propylene glycol)-*block*-poly(ethylene glycol)-*block*-poly(propylene glycol) (PPG-*b*-PEG-*b*-PPG, MW=2000), 2,4-toluene diisocyanate (TDI, 99%), Aniline (99%), Multi wall carbon nanotubes (MWCNTs, L = 10– 30  $\mu$ m and D = 10–20 nm), ammonium bicarbonate (NH<sub>4</sub>HCO<sub>3</sub>), Ethanol, Potassium Dichromate (K<sub>2</sub>Cr<sub>2</sub>O<sub>7</sub>), Hydrochloric Acid (HCl), Tetrahydrofuran (THF, 99.5%). All these chemicals were purchased from Sigma Aldrich, while THF was acquired from Merck.

### 2.2 Synthesis of PU polymer and f-CNTs@PU composite

PU was fabricated via an addition polymerization approach as reported in Sattar et al.<sup>18</sup>. In brief, two polyols (PPG-*b*-PEG-*b*- PPG and PEO) with the ratio of 0.9:0.1 were taken in THF solvent (30mL) and stirred for 1 hr at 40 °C. Afterward, 2,4-TDI (1.5 mL) was poured to polyols dropwise and the mixture was allowed to stir for 3 hrs to obtain the PU solution. The THF solvent was evaporated at ambient temperature to form PU film (1  $\pm$  0.05 mm thickness).

CNTs were purified and amine functionalized to form f-CNTs according to our previous protocol<sup>18</sup>. For Purification CNTs were annealed at 400 °C for 0.5 hr in a furnace and then refluxed in an aqueous HCl (2% w/v) for 1 hr. Finally, CNTs were filtered and washed with distilled water in order to remove the excess HCl. Filtered CNTs were oven dried at 60 °C for 10 hrs and were used for (NH<sub>2</sub>-) amine functionalization. For this purpose, MWCNTs were mixed with NH<sub>4</sub>HCO<sub>3</sub> (in a w/w ratio of 1:3) and sonicated in ethanol for 3 hrs. The mixture was dried at room temperature with constant stirring. Then the sample was ball-milled at 250 rpm for 4 hrs followed by heating at 100 °C for 24 hrs to remove the residual gases. The obtained amine modified carbon nanotubes were labeled as f-CNTs and further used in the preparation of f-CNTs@PU and PANI/f-CNTs@PU composites.

For the preparation of f- CNTs@PU composite, 0.1g of



CNTs was added to THF solvent and sonicated for 1 hr, labelled as soln-1. Moreover, PU was dispersed in THF and the resulting solution was labeled as soln-2. For composite preparation, 3.0 wt. % solution of f-CNTs was poured into the PU solution in THF solvent. Both these solutions were stirred for 12 hrs at 40 °C for better dispersion of f-CNTs in PU matrix. Finally, the product formed was poured in a glass Petri dish and the solvent was evaporated at 30 °C leaving a thin film of f-CNTs@PU composite (thickness of  $1 \pm 0.05$  mm), which was stored for further analysis.

### 2.3 Synthesis of PANI/f-CNTs@PU Composites

PANI was synthesized via single-step oxidative polymerization of aniline by using  $K_2Cr_2O_7$  and HCl as an oxidative reagent<sup>18</sup> while the fabrication of (PANI/f-CNTs@PU) composite was achieved by the combination of both solution blending and chemical in-situ polymerization methods. For this purpose, 0.1 g of f-CNTs and four weight fractions of PANI (0.1, 0.3, 0.5 and 1%) were dissolved in 20 mL of THF solvent and sonicated for 1 hr at ambient temperature. Then, PANI/f-CNTs hybrid of each concentration was poured into the PU solution and the reaction mixture was allowed to stir for 12 hrs at 40 °C. Finally, the product formed was poured in a Petri dish and solvent dried by evaporation at 25 °C leaving a thin film of PANI/f-CNTs@PU composite (thickness of  $1 \pm 0.05$  mm). Schematic structure of interaction between PANI, f-CNTs and PU in a ternary composite is shown in Scheme 1, while the synthesis scheme has been illustrated in the fig 1.

### 2.4 Characterization

For functional group analysis of PU nanocomposites (PANI/f-CNTs@PU), Infrared (IR) spectra were recorded in transmission mode on the Nexus 870 FTIR spectrometer with a scan range of 4000–450  $cm^{-1}$ . Morphological analysis of the fabricated samples was accomplished using a Hitachi S-4800 Scanning Electron Microscope (SEM).

Stress-strain behavior of fabricated composites was evaluated via a universal testing machine (UTM) (Instron 4466) according to ASTM D638 standard method under a strain rate of 5 mm/min at 23 °C. To evaluate the thermal stability of the fabricated materials, Thermogravimetric Analysis (TGA) was performed on a NETZSCH STA 449 C thermal analyzer. 7–10 mg of as-synthesized composite was taken in an  $Al_2O_3$  crucible in the temperature range of 25–700 °C with a ramping rate of 20 °C/min under nitrogen atmosphere. To investigate the phase transitions of the PU and its PANI-based polymeric films, Differential Scanning Calorimetry (DSC) was done using a Perkin–Elmer Pyris 1 DSC (Boston, MA, USA) by taking 5–7 mg of fabricated samples and using a heating rate of 10 °C/min in the temperature range of 50–100 °C under an argon atmosphere. To carry out the crystallographic analysis, X-Ray Diffraction (XRD) analysis was performed on a Shimadzu XRD-6000 utilizing crystal monochromatic  $Cu K\alpha$  radiations in the range of  $10^\circ < 2\theta < 70^\circ$  at a scan rate of 8°/min. The electrical conductivity of composite films was investigated at 25°C using the four-point technique (Keithley 2400) and rectangular films with dimensions of  $35 \times 10 \times$

$1 \pm 0.05$  mm<sup>3</sup> were employed to measure the conductivity according to ASTM D257. By using the Van der Pauw method, the probe, the resistivity of the testing material was calculated as follows:

$$\rho = \frac{V}{I} \times k \quad (1)$$

where, k is the geometry-dependent correction factor and is given as:

$$k = \frac{A}{\ell} \quad (2)$$

Where  $\rho$  shows the resistivity ( $\Omega$  cm) of the material, w (cm) is the width of the film,  $\ell$  (cm) is the space between two probes and t (cm) is the film thickness. Knowing the value of resistivity ( $\rho$ ), the conductivity can be determined as:

$$\sigma = \frac{1}{\rho} \quad (3)$$

Here,  $\sigma$  represents the electrical conductivity ( $S$  cm<sup>-1</sup>) of the material under the test.

The shape recovery (SR) effect of rectangular films with dimensions of  $35 \times 10 \times 1 \pm 0.05$  mm<sup>3</sup> was examined by bending the composite films at transition temperature ( $T_{trans}$ ) followed by cooling at 20 °C to gain temporary shape and finally reheating it. The value of  $T_{trans}$  for shape memory polyurethane and its ternary nanocomposites was observed at 60 °C, corresponding to  $T_m$  obtained from DSC analysis. The shape fixity and recovery were measured from the following equations 4 and 5.

$$\text{Shape fixation ratio} = \left( \frac{\theta_{fixed}}{\theta_{max}} \right) \times 100 \quad (4)$$

$$\text{Shape recovery ratio} = \left( \frac{\theta_{max} - \theta_i}{\theta_{max}} \right) \times 100 \quad (5)$$

Where,  $\theta$  in degrees demonstrates the angle between a line joining the midpoint and end of the curved strips and the tangential line at the midpoint of the composite films.

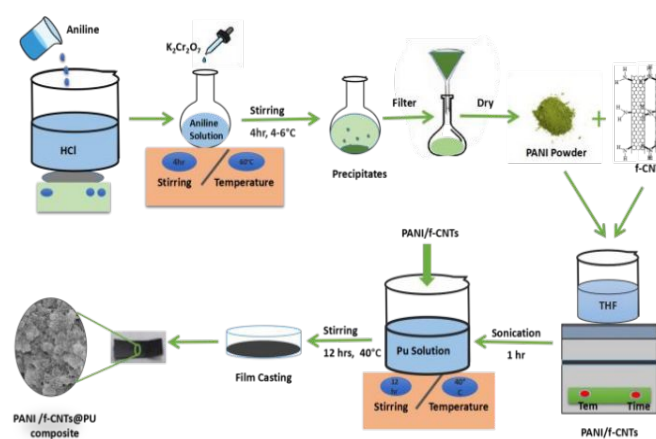
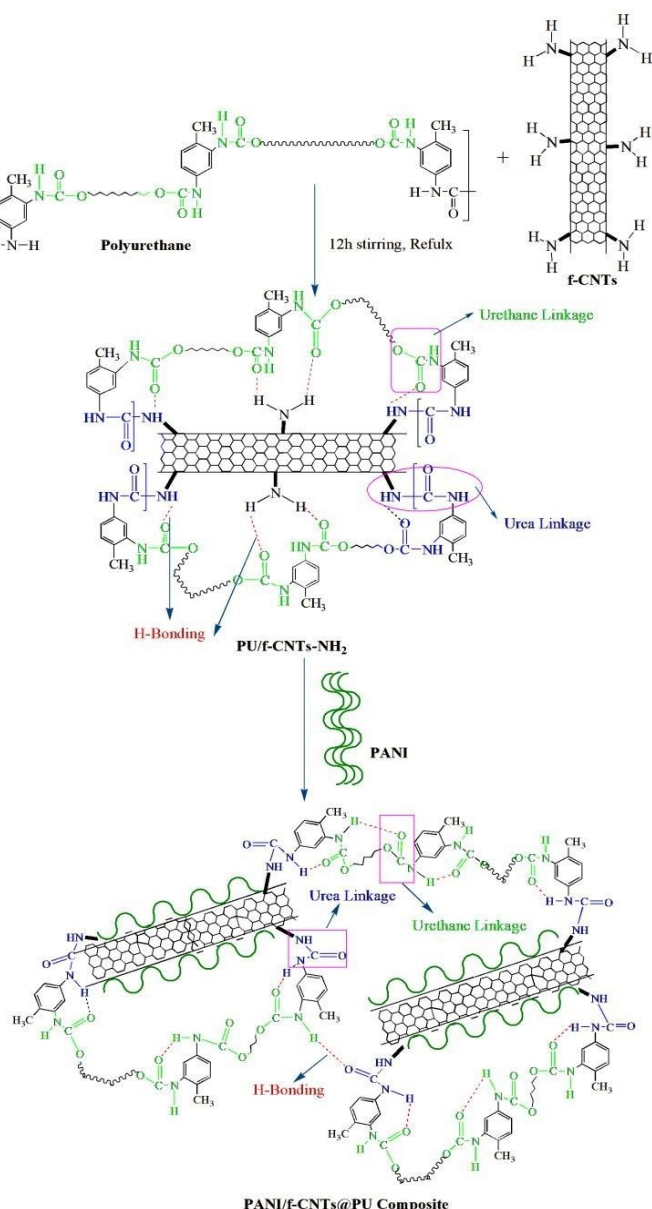


Figure 1 A schematic presentation of synthesis protocol followed for the fabrication of PANI/f-CNTs@PU nanocomposite.





Scheme 1 Probable mechanism of dispersion of PANI and f-CNTs in PANI/f-CNTs@PU composite

### 3 Results and Discussion

#### 3.1 Fourier Transform Infrared (FTIR) Spectroscopic Analysis

The FTIR spectrum of the synthesized PU and its composites is depicted in Figure 2. The band of medium intensity appeared at  $3430\text{--}3250\text{ cm}^{-1}$  is due to stretching vibrations of N—H group. Another distinctive intense band of urethane groups appears at  $1720\text{ cm}^{-1}$  and corresponds to carbonyl (C=O) stretching. Two peaks at  $1539\text{ cm}^{-1}$  and  $1022\text{ cm}^{-1}$  are credited to the bending vibration of N—H group and C—O—C bond. The peak of medium intensity appeared in the region of  $1235\text{ cm}^{-1}$  show the stretching vibration mode of C—N groups. So, these peaks for C—N, C=O and N—H groups correspond to

the presence of urethane units (i.e., —NHCOO) in the synthesized product<sup>19</sup>. Moreover, the presence of isocyanate weak band at  $2353\text{ cm}^{-1}$  indicates the NCO terminated PU chains<sup>20</sup>. The remaining peaks in the spectra are ascribed to the presence of TDI, PPG-PEG-PPG and PEO structures in the backbone of PU polymer. Details of these peaks are given in Table S1.

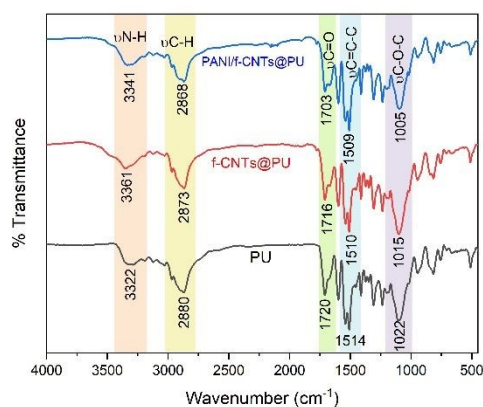
The FTIR spectrum (Fig S1) of amine functionalized CNTs shows a weak band at  $3648\text{--}3334\text{ cm}^{-1}$  due to N—H stretching. A broad band at  $1237\text{ cm}^{-1}$  indicates C—N stretching of C—NH<sub>2</sub>. These results confirm NH<sub>2</sub> groups on CNTs' surface. The FTIR spectrum of f-CNT@PU, shows that incorporation of amine functionalized CNTs in PU polymer resulted in the formation of urea linkages in addition to the urethane linkages which is ascribed to a slight increase in intensity of bands arising from the stretching vibrations of N—H and C=O groups at  $3361\text{ cm}^{-1}$  and  $1716\text{ cm}^{-1}$  respectively. This increase in the peak intensities and the appearance of shoulder peak at lower wavelength indicate the formation of new urea linkages and H-bonded N—H and C=O stretching vibrations. Absence of NCO band also supports the formation of urea bonds between NCO groups of PU and NH<sub>2</sub> groups present on the wall of f-CNTs.<sup>21</sup>

The primary FTIR characteristic bands of PANI/f-CNTs@PU composite are analogous to the f-CNTs@PU composite spectrum with a small shifting of characteristic urethane-urea peaks. The N—H and free carbonyl (C=O) stretching vibration appeared at lower frequency values i.e.,  $3332\text{ cm}^{-1}$  and  $1707\text{ cm}^{-1}$  respectively. This shift in intensities of N—H and C=O stretching vibrations suggest that interaction between PANI and PU chains is suppressed due to the presence of f-CNTs. The hydrogen bonded carbonyl (C=O) stretching vibration peak also shifted relatively towards lower frequency at  $1673\text{ cm}^{-1}$  which may indicate the presence of H-bonded urethane-carbonyl vibration and is responsible for the effective interaction among all three moieties<sup>22</sup>. Predominantly, all other characteristic bands of the pure PU, f-CNT@PU and PANI/f-CNT@PU with their characteristic frequencies are summarized in Table S1. The presence of these bands at various specified intensity values are in a good agreement with the FTIR results of PU, f-CNTs and PANI which reveals successful formation of the PANI/f-CNT@PU ternary composite.

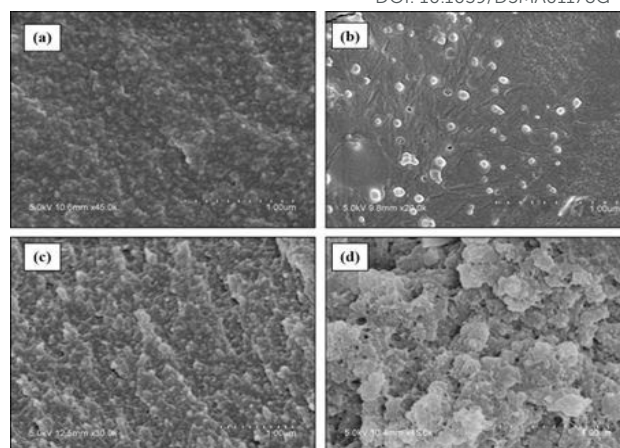
#### 3.2 Morphological Investigation

Figure 3 and (Fig S2) show the SEM microphotographs of pristine PU, f-CNTs@PU, 0.1% PANI/f-CNTs@PU composite and 1.0% PANI/f-CNTs@PU composite(s). Fig. 3(a) reveals the homogeneous surface of pristine PU and is defined as a smooth fracture<sup>23</sup> while Fig 3 b clearly shows that f-CNTs are uniformly distributed in the polymeric matrix. The polymer-integrated CNTs are shown as bright dots in the micrographs. Furthermore, it is noteworthy here that there was no aggregation in the composite, which is an outcome of amine crafting on the CNTs that offers the stronger interaction between nanotubes and matrix<sup>24</sup>. The amine groups seemed to stabilize the nanotube dispersion by developing urea linkages with the —NCO groups





2 FTIR spectrum of PANI/f-CNTs@PU composite



3 SEM images of: (a) PU; (b) f-CNT@PU; (c) 0.1% PANI/f-CNTs@PU; (d) 1.0% PANI/f-CNTs@PU at 1 μm.

present in the PU matrix. Elemental analysis (Fig S3) also confirms the presence of C, N, and O with a weight ratio of 67.27, 18.21 and 14.53 respectively, further strengthening the evidence for the presence of the NCO group. This quite fine distribution of the f-CNTs is credited to the chemical (urea linkages) and physical (hydrogen bonding) interactions between the modified nanotubes and the polymer matrix, as depicted in the proposed reaction mechanism (Scheme 1).

It is a known fact that the presence of an agglomeration of the nanofiller in the matrix depreciates the thermal and mechanical properties of the nano-composites. Here, the quite well dispersion of f-CNTs in the PU matrix can offer improved mechanical, thermal and shape memory properties to PU matrix.

The SEM micrograph of PANI/f-CNTs@PU composite with the 0.1 and 1.0 wt. % of PANI is shown in Figure 3 (c and d). It was revealed that the insertion of PANI created a short tubule-like structure with a flaky appearance, which could be uniformly dispersed in the PU polymeric matrix. Moreover, the fracture surface of polymeric matrix was found to be more rough, entangled and more flaky with an increase in concentration of PANI from 0.1% to 1.0% in the PANI/f-CNTs@PU composite<sup>23</sup>. This fractured surface is accountable for the mechanical strength of the fabricated nanocomposite<sup>25</sup> and validates the results of mechanical strength as shown in figure 4 (mechanical strength).

### 3.3 Stress-Strain Analysis

The impact of PANI concentration on ultimate tensile strength and Young's modulus of f-CNTs@PU based ternary composites is depicted in fig 4. The mechanical properties for pristine PU strips were poor owing to the presence of entangled polyol soft segment<sup>26</sup>. However, the addition of f-CNTs into the PU matrix enhanced the Young's modulus and tensile strength of the PU matrix<sup>27</sup>. On the addition of 3 wt. % of f-CNTs in the PU matrix, the tensile strength and Young's modulus of composite was increased from  $16.36 \pm 0.49$  MPa in pure PU to  $21.16 \pm 0.63$  MPa (an increase of 29%) and  $299.29 \pm 8.98$  to  $423.79 \pm 12.71$  MPa (an increase of 42%), respectively. The

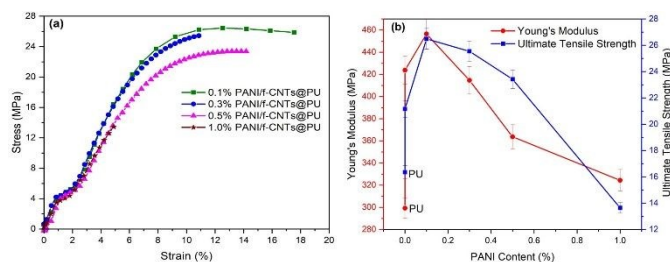
improved mechanical properties of this binary composite can be credited to the strong interfacial interaction of f-CNTs with the PU chains<sup>28</sup>. Additionally, the amine functional group on the CNTs is also helpful in the formation of urea linkages<sup>29</sup>. Therefore, these interactions between the f-CNTs and the PU matrix significantly improved the dispersion as well as the interfacial adhesion, resulting in strengthening of the overall mechanical performance of the nanocomposite<sup>28</sup>.

In the case of PANI/f-CNTs@PU composites, incorporation of 0.1 wt.% PANI content to the f-CNT@PU resulted in an increase of about 53% in Young's modulus and 50% in tensile strength values compared to the neat one. The improved mechanical strength of the nanocomposite can be ascribed to the well dispersal of PANI content in the f-CNT@PU matrix as well as strong interfacial interaction between PANI and the f-CNT@PU polymer matrix. However, for the sample with higher content of PANI (1.0% PANI/f-CNTs@PU), lower values for tensile strength ( $13.65 \pm 0.41$  MPa) and Young's modulus ( $324.44 \pm 9.73$  MPa) were determined. The observed decrease in the material's strength is due to the presence of agglomerates in these composites, resulting from the layered adsorption of PANI chains on the nanotubes wall and less interaction of f-CNTs with the PU matrix<sup>20</sup>. The stress-strain properties of the PU polymer, f-CNTs@PU and PANI/f-CNTs@PU nanocomposite(s) calculated from stress-strain values are summarized in Table S2.

### 3.4 Thermogravimetric Analysis

The effect of f-CNTs and PANI filler on the thermal stability of PU matrix was examined via TGA as shown in figure 5. The energy of covalent bonds that constitute the polymeric network in a polymer matrix as well as chemical/physical interaction among the filler and polymeric matrix are the fundamental factors that influence thermal stability of the nanocomposite<sup>30</sup>. All TGA curves comprising neat PU and its nanocomposite(s) showed a two-stage degradation due to the soft and hard segments in PU. The maximum





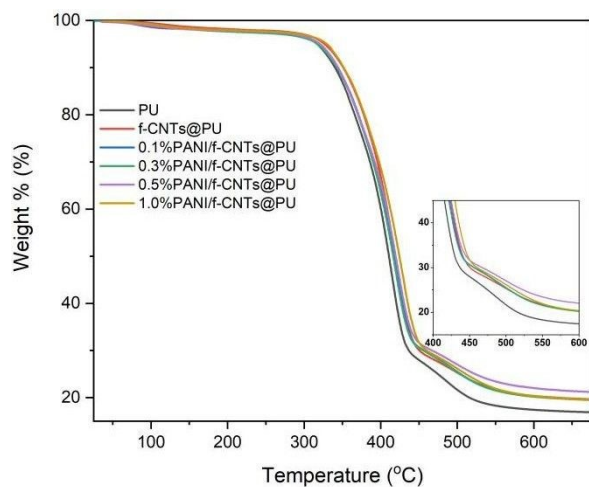
4 Impact of PANI concentration on: (a) Ultimate tensile strength; (b) Young's modulus of f-CNTs@PU based ternary composites

degradation temperature for the first and second stage of pristine PU were around 410 and 482 °C, while those of f-CNTs@PU nanocomposite were at 413 and 486 °C, respectively (Table S3). This increase in degradation temperature for nanocomposite can be ascribed to f-CNT interaction with PU and decreased PU chain's thermal motion<sup>27</sup>.

Furthermore it was revealed that PANI insertion to f-CNT@PU also enhanced the degradation temperature of the polymeric matrix in PANI/f-CNTs@PU. Similarly, an increase in onset temperature up to 342°C was observed with the increase of PANI concentration from 0.1 to 1.0 wt. %, which can be ascribed to the combined effect of f-CNTs and PANI capitalizing the presence of interfacial and H-bonding in the PU based ternary polymeric material<sup>31</sup>. Additionally, higher char residue was also found for the nanocomposite which may offer higher thermal stability as revealed by many studies in the literature<sup>32, 33</sup>.

### 3.5 Differential Scanning Calorimetry

The DSC heating and cooling traces of PU and its nanocomposite are displayed in Figure 6(a & b), respectively. The melting temperature ( $T_m$ ), glass transition temperature ( $T_g$ ), crystallization temperature ( $T_c$ ), heat of crystallization ( $\Delta H_c$ ) and heat of melting ( $\Delta H_m$ ) obtained from DSC analysis are summarized in Table 4S.



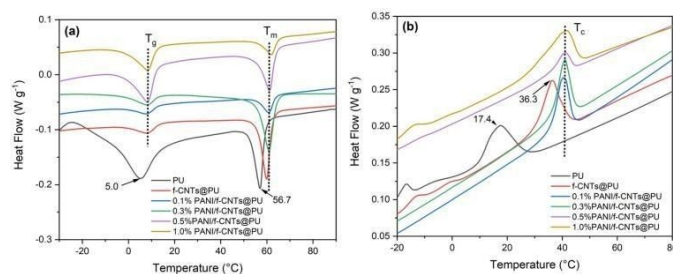
5 TGA Curves for PU, f-CNTs@PU and PANI/f-CNTs@PU composite films

It was observed that melting and crystallization temperatures increased with the addition of f-CNTs into the PU matrix. Melting temperature for the neat PU appeared at around 57 °C and only 2 °C rises in  $T_m$  was determined for the f-CNTs@PU nanocomposite. Yet, a considerable shift was ascertained in crystallization behavior. As the incorporation of f-CNTs in the PU matrix results in the rise of about 18 °C in crystallization temperature in comparison to neat PU. This was ascribed to H-bonding (—NH groups from the urethane linkages with the >C=O group of the hard segments or with the —O— of the soft segments) and urea linkages (between —NH<sub>2</sub> from f-CNTs and —NCO of PU). Besides this nucleating outcome of f-CNTs in the composite is also evident from the rise in  $T_c$  and  $T_m$  (Figure 6a). Furthermore, the melt as well as crystallization enthalpies for the nanocomposite were also enhanced compared to pure PU. These findings indicated that the cross-linking was also responsible for an increase in  $T_g$  of f-CNTs@PU as displayed in Figure 6. Well dispersion of f-CNTs in the PU matrix may hinder the molecular motion of polymeric chains, which could be responsible for an increased  $T_g$  of nanocomposite<sup>19</sup>.

In the case of PANI/f-CNTs@PU composites, the incorporation of PANI increased the melting and crystallization temperatures in composites at a lower loading. The effect was more significant in the composite having 0.1% PANI (0.1 %PANI/f-CNTs@PU). The highest value of  $T_g$  was also obtained for the nanocomposite with 0.1% PANI as shown in Figure 6. Further increase in the polyaniline content up to 1.0 wt. % resulted in a decrease in  $T_m$ ,  $T_c$ ,  $T_g$  and lower heat of melting as well as crystallization. This may be ascribed to the surface overlapping of PANI chains on the walls of f-CNTs and less interaction of PANI with PU matrix. This could increase the PU chains' flexibility and phase incompatibility, which in turn are responsible for the decreased DSC parameters with the higher loading of PANI in nanocomposites.

### 3.3 X-Ray Diffraction

Figure 7 depicts the XRD patterns of PU, f-CNTs@PU and PANI/f-CNTs@PU nanocomposites. PU has a broad but a low intensity peak in the form of a hump with a maximum at 21° (2 $\theta$ ) corresponding to (110) indices which reveals its slight amorphous nature. This amorphous nature is a result of the randomized orientation of methyl groups connected to PU linkages in the pristine PU<sup>34, 35</sup>. It is clear from Figure 7(b) that the incorporation



6 DSC thermograms showing: (a) melting temperature ( $T_m$ ); (b) crystallization temperature ( $T_c$ ); (c) glass transition temperature ( $T_g$ ) for PU, f-CNTs@PU and PANI/f-CNTs@PU composite films



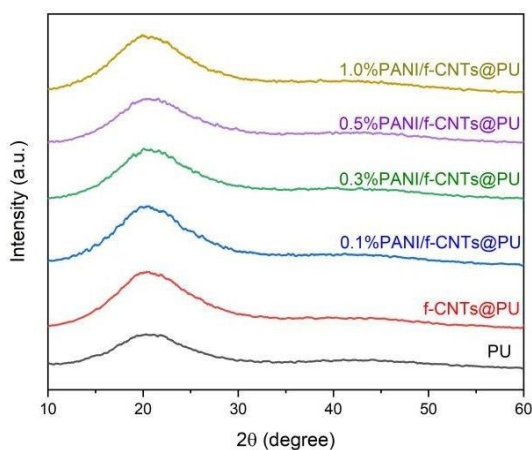


Figure 7 XRD patterns for PU, f-CNT@PU, and PANI/f-CNTs@PU composite (0.1, 0.3, 0.5 and 1.0% loading of PANI)

of f-CNTs improved the crystallinity of the PU. Though position of the PU peak remained unchanged but the intensity of the hump is slightly increased, which can be credited to the nucleation effect of f-CNTs<sup>34</sup>.

All four concentrations of PANI/f-CNTs@PU composite (0.1, 0.3, 0.5 and 1.0%) also showed a broader and weaker peak (21°) at a similar position as observed in the pristine PU and f-CNTs@PU which reveals that insertion of PANI did not affect the position of the crystallographic plane (110) of the PU. However, a slight increase in peak intensity was observed with an increase in concentration of PANI which is due to the semi-crystalline nature of PANI<sup>36</sup>. Hence, this semi-crystalline nature of PANI showed a slight improvement in the structure of f-CNTs@PU which can offer improved electrical and thermal properties<sup>31, 37</sup>.

### 3.3 Electrical Conductivity Measurement

The influence of f-CNTs and PANI on the electrical conductivity of the fabricated PU films was examined and the results are demonstrated in Table 5S. For the PU

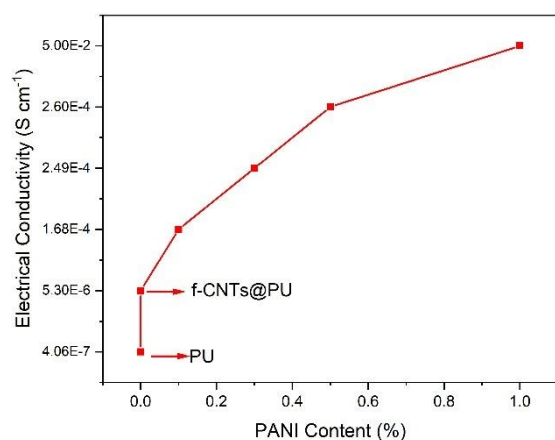


Figure 8 The impact of PANI concentration on electrical conductivity of pristine PU in PANI/f-CNTs@PU composite films

matrix alone,

the electrical conductivity was  $4.06 \times 10^{-7} \text{ S cm}^{-1}$ , and it raised to  $5.30 \times 10^{-6} \text{ S cm}^{-1}$  by the insertion of f-CNTs. This value is in the range of  $10^{-6} \text{ S cm}^{-1}$  which is a prerequisite for the antistatic properties of the materials for various applications<sup>38</sup>. This improvement in the electrical conductivity of the nanocomposite on loading f-CNTs is ascribed to the well dispersion of nanotubes that resulted in a conductivity network formation in the PU matrix.

For PANI/f-CNTs@PU composites, the electrical conductivity values were found in the range between  $1.68 \times 10^{-4}$  and  $5.00 \times 10^{-2} \text{ S cm}^{-1}$  on addition of 0.1-1.0 wt. % of PANI. The impact of PANI content on PANI/f-CNTs@PU nanocomposites is displayed in Figure 8 (b). These values are in the range of  $10^{-4}$ – $10^{-2} \text{ S cm}^{-1}$  suggesting the formation of conductive networks that are a prerequisite for electromagnetic shielding (EMI) based applications as reported in the literature<sup>39, 40</sup>. The improved conductivity of nanocomposite films is credited to the formation of conductive PANI chains over the nanotubes interconnected phase in the insulating PU matrix and it is in good agreement with the morphological structure as depicted in the SEM micrograph of Figure 4 (d). The 1.0% PANI/f-CNTs@PU composite revealed a higher value of conductivity ( $5.00 \times 10^{-2} \text{ S cm}^{-1}$ ) compared to other nanocomposite films, which indicates a 100-fold increase. Hence, it was found that increased content of PANI into PU matrix reinforced the conducting bridges in the f-CNT@PU hybrid, which leads to the improved electrical conductivity.

### 3.8 Shape Memory Study

To evaluate the shape memory properties (i.e., shape recovery and shape fixity), PU-based films were bent at the transition temperature ( $T_{\text{trans}}$ ) and then cooled at ambient temperature (20 °C) to gain temporary shape and lastly heated again. The value of  $T_{\text{trans}}$  for pure PU and its nanocomposite was around 60 °C, revealing the  $T_m$  values shown from DSC analysis. Since the glass transition temperature is low and difficult to control at  $T_g$ , this shape memory belongs to  $T_m$ -type<sup>18</sup>. The PU and f-CNTs@PU nanocomposite showed a prompt response to recover its original shape within 60 sec as listed in the Table 5S.

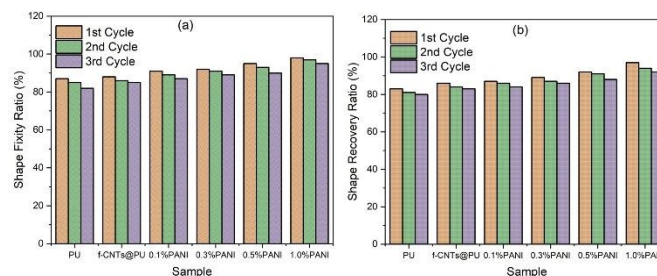


Figure 9 The impact of PANI concentration on shape fixity and shape recovery of pristine PU in PANI/f-CNTs@PU composite films over three cycles



For pure PU, 87% shape fixity was determined during the first cycle while shape memory fixity of 88% was appeared for f-CNTs@PU nanocomposite as depicted in Figure 9 (a). The nanocomposites of PANI/f-CNT@PU showed higher shape fixity as compared to pure PU and f-CNT@PU. For 0.1%PANI/f-CNT@PU, 91% shape fixity was determined while maximum shape fixity (98%) was achieved for 1.0%PANI/f-CNT@PU (1.0 wt. % PANI). During the second cycle, shape fixity values were reduced to 85, 86, 89, 91, 93, and 97 while for the third heating cycle, a further decrease in shape fixity was found in order of 82,85,87, 89,90, and 95 for pure PU, f-CNT@PU, 0.1%PANI/f-CNT@PU, 0.3%PANI/f-CNT@PU, 0.5%PANI/f-CNT@PU, and 1.0%PANI/f-CNT@PU respectively. The results of shape fixity values of all PU-based films over three heating cycles are shown in Figure 9 (b).

Additionally, similar increasing shape recovery results were achieved with the addition of PANI to the PU matrix. Figure 9 b shows the shape recovery properties of all the fabricated films over three heating cycles. For pristine PU, 83.0% shape recovery was determined while shape memory recovery of 86% was appeared for f-CNTs@PU nanocomposite during the first heating cycle as depicted in Figure 9b. It is clear that CNTs incorporation enhanced the shape recovery of the PU chains by developing urea linkages and H-bonding<sup>41</sup>.

The nanocomposites of PANI/f-CNT@PU showed higher shape recovery values as compared to pristine PU and f-CNT@PU. For 0.1%PANI/f-CNT@PU, 87% shape recovery was determined while maximum shape recovery (97%) was appeared for 1.0%PANI/f-CNT@PU (1.0 wt. % PANI) as shown in Figure 9 B and 10 (C & D). It is obvious that the integration of PANI along with f-CNTs led to a considerable improvement in shape memory due to layered adsorption of PANI chains on the surface of f-CNT@PU and strengthened the polymer networks *via* chemical and physical interactions. Accordingly, a high degree of soft segment's crystallinity contributes to higher electrical conductivity which in turn offers a high shape recovery performance of composites. Furthermore, during the second cycle, shape recovery values were found to be 81, 84, 86,87,91, and 94 %, while for the third heating cycle, shape memory percentage was found to be 80, 83, 84, 86, 88, and 92 for pure PU, f-CNT@PU, 0.1%PANI/f-CNT@PU, 0.3%PANI/f-CNT@PU, 0.5%PANI/f-CNT@PU, and 1.0%PANI/f-CNT@PU respectively.

These three cycle shape fixity and shape recovery results indicates that PANI/f-CNT@PU films retain a higher shape memory performance with only a 3% reduction in shape fixity and 5% reduction in shape recovery, showing excellent cycle to cycle stability. This minor reduction can be indicative of polymeric chain rearrangements and stress relaxation during repeated heating cycles.

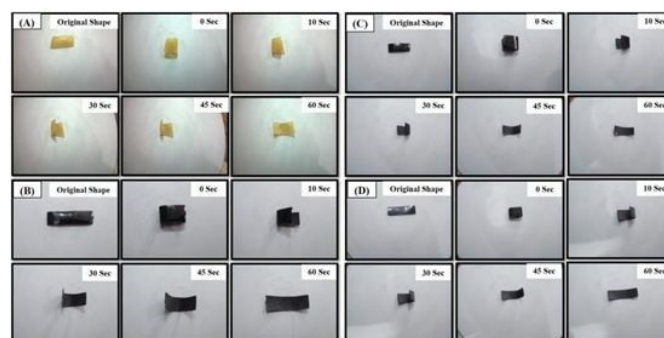


Figure 10 Shape memory recovery of: (A)PU; (B)f-CNT@PU; (C) 0.1%PANI/f-CNT@PU; (D) 1.0%PANI/f-CNT@PU

## Conclusions

In the current work, we designed a PU based ternary composite via a facile solution blending approach that has homogeneous morphology due to the fine dispersion of modified nanotubes attributing the formation of urea linkages (reaction N–H of PANI and –NCO of PU), which accounts for the improved mechanical properties and degradation temperature. The fabricated composite film fruitfully attained the coexistence among electrical performance, shape recovery and shape fixity to a desirable extent for its practical utility. The DSC studies revealed that the addition of PANI up to 1.0 wt. % increased the  $T_g$ ,  $T_m$  and  $T_c$  owing to cross-linking along with chain rigidity. Excellent shape recovery effect of about 97 % was determined in the composite (1.0%PANI/f-CNTs@PU) which demonstrated that higher PANI content improved the shape memory capability of the PU matrix. The prepared nanocomposites with significant shape recoverability and electrical conductivity values in the range of  $10^{-6}$ - $10^{-2}$  S  $cm^{-1}$  could lead to an excellent performance at an industrial scale for a variety of applications, including sensors, self-healing materials and electronics etc.

## Author contributions

T.I and R.S conceptualization, methodology, original draft writing and writing—review and editing. R. N and S.U. : conceptualization, methodology, review and editing. R. S: Investigation, Formal Analysis. T.I.: investigation, supervision and supporting. M.I. : writing, visualization and software. T. I.: visualization and software. R.S and R.N: conceptualization, supervision, review and editing.

## Conflicts of interest

There are no conflicts to declare.

## Data availability

Data will be made available on request.



## Acknowledgements

No funding was received for this study.

## References

- L. Luo, F. Zhang, L. Wang, Y. Liu and J. Leng, *Advanced Functional Materials*, 2024, **34**, 2312036.
- L. Luo, F. Zhang and J. Leng, *Composites Science and Technology*, 2021, **213**, 108899.
- H.-X. Wang, X.-Y. Zhao, J.-Q. Jiang, Z.-T. Liu, Z.-W. Liu and G. Li, *ACS Applied Materials & Interfaces*, 2022, **14**, 51244- 51252.
- S. Zhao, Y. Fan, R. Yang, Z. Ye, F. Zhang, C. Wang, W. Luo, Y. Wen and J. Zhou, *Opto-Electronic Advances*, 2025, **8**, 240109-240101-240109-240109.
- X. Xiao, D. Kong, X. Qiu, W. Zhang, F. Zhang, L. Liu, Y. Liu, S. Zhang, Y. Hu and J. Leng, *Macromolecules*, 2015, **48**, 3582- 3589.
- X. Du, F. Zhang, L. Hu, L. Luo, Z. Liu, Y. Liu and J. Leng, *Composites Part A: Applied Science and Manufacturing*, 2025, **190**, 108595.
- V. Aswany, R. Parvathy, D. Mottammal, S. A. Thomas, J. Cherusseri, D. Kumar, A. Kumar and D. N. Rajendran, in *Polymer Nanocomposites for 3D, 4D and 5D Printing: Fundamental to Applications*, Springer, 2025, pp. 213-240.
- Senyurt, M. A., Kurdis, M. M., Ulus, H., & Avci, A., *Fibers and Polymers*, 2025, **26**, 2097-2116.
- L. Chen, Z. Xu, M. Gong, L. Zhang, D. Wang, H. Zhou and X. Lin, *Chemical Engineering Journal*, 2025, **510**, 161504.
- S. Gopinath, N. N. Adarsh, P. Radhakrishnan Nair and S. Mathew, *Polymer Composites*, 2023, **44**, 4433-4458.
- R. Sanaka and S. K. Sahu, *Heliyon*, 2024, **10**.
- M. Babar, A. Sharma, P. Kakkar, A. Arora, T. Arora and G. Verma, *Progress in Organic Coatings*, 2022, **165**, 106743.
- G. A. Gohar, A. Akhtar, H. Raza, G. Mustafa, M. Fatima, H. U. Rehman, M. W. Aslam, A. ul Haq and W. Manzoor, *Nano Express*, 2023, **4**, 045013.
- S. Namathoti and M. R. K. Vakkalagadda, *Polymers*, 2023, **15**, 710.
- H. Du, S. Liu, F. You, J. Wang, Z. Ren and Z. Wu, *Progress in Natural Science: Materials International*, 2021, **31**, 557-566.
- A. Zotti, S. Aprano, A. Rafiq, S. Zuppolini, M. Zarrelli, M. G. Maglione, P. Tassini, A. Cassinese and A. Borriello, *Materials Advances*, 2025, **6**, 1788-1793.
- H.-Y. Wang, D. Liu, K. Zhang, C. Qian, Y. Dong, N. Jamaluddin, J. Matmin and Y. Zhu, *Journal of Alloys and Compounds*, 2025, 181930.
- R. Sattar, A. Kausar and M. Siddiq, *Chinese Journal of Polymer Science*, 2015, **33**, 1313-1324.
- Y. Yin, C. Guo, W. Li, H. Liu and Q. Mu, *Composites Communications*, 2024, **50**, 102017.
- Z. Yan, Y. Liu, Y. Cao, G. Quan, W. Li, D. Li, Y. Wu, L. Xiao and F. Yu, *Journal of Applied Polymer Science*, 2024, **141**, e55653. New Article Online  
DOI: 10.1039/D5MA01178G
- R. Wang, H. Wu, R. Chen and Y. Chi, *Small*, 2019, **15**, 1901550.
- K. Baidya, A. Roy and K. Das, *Materials Today Communications*, 2025, **47**, 112979.
- X.-Z. Tian, R. Yang, J.-J. Ma, Y.-H. Ni, H.-B. Deng, L. Dai, J.-J. Tan, M.-Y. Zhang and X. Jiang, *Chinese Journal of Polymer Science*, 2022, **40**, 789-798.
- M. Sabet, *Polymer-Plastics Technology and Materials*, 2025, **64**, 465-494.
- Y. H. Jo, H. Jung, S. Jeon, H. Choi, H.-W. Kim and H. Sung, *Journal of Materials Research and Technology*, 2025, **36**, 5696-5706.
- Y. Liu, J. Li, L. Jia, M. Li, Y. Diao, Z. Han, C. Yu and T. Liu, *Materials & Design*, 2025, **250**, 113611.
- M. Bidshahri, A. Ameri, M. Sharif and A. Ranjbar, *International Journal of Polymer Science*, 2025, **2025**, 4505715.
- G. Neeraja Rani, R. Panthagani and M. Kanaka Durga, *Materials Research Innovations*, 2025, **29**, 129-134.
- S. Zhang, Y. Xiong, Y. Wang, Y. Ma, J. Li, C. Jiang, C. Wang, Y. Zhu, Y. Zhao and G. Zhang, *Polymer International*, 2024, **73**, 874-882.
- Y. Yao, S. Jin, X. Ma, R. Yu, H. Zou, H. Wang, X. Lv and Q. Shu, *Composites Science and Technology*, 2020, **200**, 108457.
- B. Gai, S. Li, J. Zhang, Z. Jiang, G. Xie, J. Zhang, S. Xing and M. Yao, *Journal of Applied Polymer Science*, 2024, **141**, e55761.
- M. Yang, T. Wang, Y. Tian, H. Zhang, J. Zhang and J. Cheng, *Green Chemistry*, 2024, **26**, 4771-4784.
- H. Chen, G. Ji, F. Lan, Z. Wang, C. Chen, J. Luan, C. Dong and Z. Lu, *International Journal of Biological Macromolecules*, 2024, **270**, 132330.
- T. C. Codau and E. Codau, *Materials Today Sustainability*, 2024, **27**, 100831.
- A. Shahzaib, S. A. Hamdani, R. Mehndi, S. Anjum, S. M. Alshehri, T. Ahamad and N. Nishat, *Inorganic Chemistry Communications*, 2025, 114644.
- S. V. Ebadi, M. Asadolahi and S. J. Mousavifard, *Microchemical Journal*, 2025, 114173.
- N. Bora, D. P. Joshi and J. S. Aulakh, *Polymer Bulletin*, 2024, **81**, 1597-1621.
- Y. Yang, L. Zhang, S. Ge, H. Huo, K. Huang, M. Rezakazemi and Z. Zhang, *Journal of Materials Chemistry A*, 2025, **13**, 15075-15087.
- M. Siri, M. Chandrashekara, B. Hareesh and K. Nandan, *Synthetic Metals*, 2025, 117937.
- M. D. Ali, A. Aslam, M. A. Haider, U. Fakhar, S. Ezzine and



## ARTICLE

## Journal Name

- H. Smaili, *Inorganic Chemistry Communications*, 2022, 146, 110039.
41. W. Liu, S. Yang, L. Huang, J. Xu and N. Zhao, *Chemical Communications*, 2022, **58**, 12399-12417

View Article Online  
DOI: 10.1039/D5MA01178G

Open Access Article. Published on 21 May 2026. Downloaded on 5/22/2026 1:44:54 AM.  
This article is licensed under a Creative Commons Attribution-NonCommercial 3.0 Unported Licence.



Materials Advances Accepted Manuscript

## Data availability statement

View Article Online  
DOI: 10.1039/D5MA01178G

The data supporting this article have been included as part of the Supplementary Information.

